

PCCP

Accepted Manuscript



This is an *Accepted Manuscript*, which has been through the Royal Society of Chemistry peer review process and has been accepted for publication.

Accepted Manuscripts are published online shortly after acceptance, before technical editing, formatting and proof reading. Using this free service, authors can make their results available to the community, in citable form, before we publish the edited article. We will replace this *Accepted Manuscript* with the edited and formatted *Advance Article* as soon as it is available.

You can find more information about *Accepted Manuscripts* in the [Information for Authors](#).

Please note that technical editing may introduce minor changes to the text and/or graphics, which may alter content. The journal's standard [Terms & Conditions](#) and the [Ethical guidelines](#) still apply. In no event shall the Royal Society of Chemistry be held responsible for any errors or omissions in this *Accepted Manuscript* or any consequences arising from the use of any information it contains.

Ultrafast Relaxation Dynamics of Phosphine-Protected, Rod-Shaped Au₂₀ Cluster: Interplay Between Solvation and Surface Trapping

Cite this: DOI: 10.1039/x0xx00000x

Received 00th January 2012,
Accepted 00th January 2012

DOI: 10.1039/x0xx00000x

www.rsc.org/

Meng Zhou,^a Saran Long,^a Xiankai Wan,^b Yang Li,^a Yingli Niu,^a Qianjin Guo,^{a*} Quan-Ming Wang^{b*} and Andong Xia^{a*}

The exact interaction between Au cores and surface ligands remains largely unknown because of the complexity of the structure and chemistry of ligand/Au-core interfaces in ligand-protected Au nanocluster (AuNCs), which are commonly found in many organic/inorganic complexes. Here, femtosecond transient absorption measurement of the excited-state dynamics of a newly synthesized phosphine-protected cluster [Au₂₀(PPhpy₂)₁₀Cl₄]Cl₂ (**1**) is reported. Intramolecular charge transfer (ICT) from the Au core to the peripheral ligands was identified. Furthermore, we found that solvation strongly affected ICT at ligand/Au-core interfaces while by choosing several typical alcoholic solvents with different intrinsic solvation times, we successfully observed that excited-state relaxation dynamics together with displacive excited coherent oscillation of Au₂₀ cluster was significantly modulated through the competition between solvation and surface trapping. The results provide a fundamental understanding of the structure–property relationships of the solvation-dependent core–shell interaction of AuNCs for the potential applications in catalysis, sensing and nanoelectronics.

1. Introduction

Ligand-protected gold nanoclusters (AuNCs), which contain an Au core and a single layer ligand shell, have received tremendous attention in the past few years because of their potential applications in catalysis, sensing and nanoelectronics.^{1–8} Ligands are generally used during the synthesis of AuNCs to control nucleation and growth and to provide chemical and colloidal stability.⁹ Because of the complexity of the structure and chemistry of ligand/Au-core interfaces, understanding the actual interaction between the Au-core and the ligand shell remains a challenge, while few studies on intramolecular charge transfer (ICT) between the Au-core and the ligand shell have been reported.^{10–13} Intensive investigation on the excited-state behavior of AuNCs with atomic precision is necessary to obtain insight into a series of fundamental physical chemistry questions regarding the catalytic behavior,¹⁴ electron-phonon coupling or acoustic breathing vibrations,^{15–17} core/shell

interactions,^{18, 19} and intra-/inter-molecular charge transfer.^{20–22}

Recently, we identified that ICT occurs from the exterior ligand shell to the interior Au-core upon excitation in a thiolate-protected Au₂₀(SR)₁₆ cluster.¹⁷ No distinguishable oscillation of Au₂₀(SR)₁₆ was observed in nonpolar cyclohexane ($\Delta f \approx 0$), while the intensity and period (time of one cycle) of the oscillation increase with increasing solvent polarity from toluene ($\Delta f = 0.0159$) to THF ($\Delta f = 0.210$), indicating optically excited oscillation could be enhanced in more polar solvent. Once the cluster is excited into highly excited states, the solvent dipoles will rearrange around the cluster dipole moment when the excess energy is transferred to the surrounding solvents, which is called solvation.²³ Unlike those large metal nanoparticles (>2 nm) in which the oscillation is dependent on excitation power,^{3, 24} oscillations of very small metal clusters are excitation-intensity-independent and are not easy to be seen because of their relatively high frequency.^{16, 17} Thus, the observed solvent-polarity-dependent oscillations suggested that the total cluster size of Au₂₀(SR)₁₆ increased in more polar solvents by absorbing external solvent molecules around the excited cluster surface because of solvation,¹⁷ which lowers the oscillation frequency. Furthermore, AuNCs are normally treated as superatoms with discrete energy levels, and relaxation from core state to surface shell (trap) state is proposed before.^{12, 13, 25–28} In our recent investigation, it is also suggested that the excited-state energy is quickly transferred to the surface trap states from the ICT state of excited AuNCs.¹⁷ Since the nature of optical excitation and the degree of ICT in AuNCs are strongly influenced by the surrounding solvents,²⁹ potential competition between solvation and surface trapping could exist, and this could seriously modulate both the excited state relaxation and oscillations in quantum sized AuNCs (<1 nm), which is the key

^aThe State Key Laboratory of Molecular Reaction Dynamics, and Beijing National Laboratory for Molecular Sciences (BNLMS), Institute of Chemistry, Chinese Academy of Sciences Beijing 100190 (China)

E-mail: andong@iccas.ac.cn; guoqj@iccas.ac.cn

^bState Key Laboratory of Physical Chemistry of Solid Surfaces, Department of Chemistry, College of Chemistry and Chemical Engineering, Xiamen University, Xiamen, Fujian 361005 (China)

E-mail: qmwang@xmu.edu.cn

Electronic Supplementary Information (ESI) available: See DOI: 10.1039/b000000x/

feature for us to understand the complicated interactions between ligand and metal-core in organic/inorganic complexes.

To explore how the competition between solvation and surface trapping modulates the excited-state behaviors of AuNCs, we performed a femtosecond transient absorption measurement on the excited-state dynamics of a newly synthesized phosphine-protected cluster $[\text{Au}_{20}(\text{PPhy}_2)_{10}\text{Cl}_4]\text{Cl}_2$ (**1**)³⁰ in a series of alcoholic solvents. The dicationic $[\text{Au}_{20}(\text{PPhy}_2)_{10}\text{Cl}_4]^{2+}$ (**A1**) (see Fig. S1 in the Supplementary Information) comprises an Au_{20} core, ten phosphines and four chloride ligands. Unlike the thiolate-protected $\text{Au}_{20}(\text{SR})_{16}$ cluster which contains a prolate shaped Au_8 core and four Au_3SR_4 motif-shaped ligands,³¹ **1** has a rod-shaped Au_{20} core viewed as two incomplete icosahedral Au_{11} sharing two Au atoms and has no surface gold atoms as in the $\text{Au}_3(\text{SR})_4$ surface motifs of $\text{Au}_{20}(\text{SR})_{16}$. Methanol, ethanol, and *n*-propanol were chosen as solvents for this study because of their similar polarities but different intrinsic solvation times (the polarity and solvation time of these solvents are listed in Table 1),²³ which allowed for direct study of the excited-state relaxation dynamics of AuNCs modulated through competition between solvation and surface trapping.

2. Experimental Methods

2.1 Materials

The synthesis of the $[\text{Au}_{20}(\text{PPhy}_2)_{10}\text{Cl}_4]\text{Cl}_2$ cluster by Wang and coworkers was reported elsewhere.³⁰ For the spectroscopic measurements, purified (stored in powder form in a dry and dark container) **1** was dissolved in proper solvents (i.e. methanol, ethanol, *n*-propanol, all were of AR-grade).

2.2 Steady State and Transient Absorption Measurements

Ultraviolet/visible (UV/vis) absorption spectra were measured on a spectrophotometer (UV1601, Shimadzu, Japan) at ambient temperature. The femtosecond transient absorption was measured with $\sim 90\text{fs}$ time-resolution using a home-built femtosecond broadband pump-probe setup. Details of the instrument have been described elsewhere.¹⁷ Briefly, a regeneratively amplified Ti:sapphire laser (Coherent Legend Elite) produced 40 fs, 1mJ pulses at a 500 Hz repetition rate at 800 nm with a bandwidth (FWHM) of about 30 nm. The output from the amplifier was split by a 90/10 beamsplitter to generate pump and probe beams. A portion of the 800 nm pulse was doubled with a 0.5 mm thick BBO (type I) crystal to provide the 400 nm pump pulse. The probe beam at 800 nm was sent to a computer-controlled optical delay line and then focused onto a 2-mm-thick water cell to generate a white light continuum which was split into two beams using a broadband 50/50 beamsplitter as the reference and signal beams.

2.3 Data Analysis

The differential absorbance $\Delta A(t, \lambda)$ was analyzed as a function of wavelength and time delay using the population dynamics modeling toolbox software developed by van Wilderen et al.³² Spectral chirp in the transient absorption spectra was corrected for group velocity dispersion of the probe beam. Singular value decomposition (SVD) analysis was performed before the global fitting to estimate the number of components and to check for structured residuals. Sequential decay path way was utilized to model the data $\Delta A(t, \lambda)$ which was a superposition of different spectral components $\varepsilon_i(\lambda)$ weighted by their concentration $c_i(t)$ ³³:

$$\Delta A(t, \lambda) = \sum_{i=1}^n c_i(t) \varepsilon_i(\lambda)$$

A sequential scheme with increasing lifetimes was used resulting in Evolution Associated Difference Spectra (EADS). Fourier transform of the kinetic data at specific wavelength was calculated in order to obtain the frequency of the acoustic vibration. The amplitude of the Fourier transform was determined by calculating the value around the peak of the vibration mode.

3. Results and discussion

3.1 Steady State Absorption

The UV-Vis steady state absorption spectra of **1** in methanol, ethanol and *n*-propanol are shown in Fig. 1. In all solvents, the absorption spectra exhibit prominent peaks around 480 nm, 350 nm (shoulder) and 260 nm. The peak around 260 nm is ascribed to the intraligand transition of the PPhy₂ ligands,³⁰ while the peaks around 480 nm and 350 nm originate from the Au core. The absorption spectrum of **1** also exhibits a very weak absorption around 600 nm, which was recently predicted by quantum chemical calculations.³⁴ Compared with thiolate ligands,^{17, 35} phosphine ligands have lower chemical potentials with stronger electron-accepting capabilities and accept electrons from the Au core.^{36, 37} To investigate the charge transfer features of **1**, quantum chemical calculations were performed using the time-dependent density functional theory (TDDFT) method.

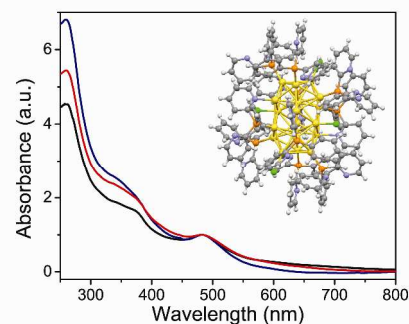


Fig. 1 Steady state absorption of **1** dissolved in methanol (black), ethanol (blue) and *n*-propanol (red). The absorbance was normalized at 480 nm. The inset shows the structure of $[\text{Au}_{20}(\text{PH}_3)_6(\text{PH}_2\text{py})_4\text{Cl}_4]^{2+}$ in **1**.

3.2 Quantum Chemical Calculation

Density function theory (DFT) was used to study the molecular orbitals, visualized transition density (TD) and charge difference density (CDD) of the phosphine protected Au_{20} cluster. The method and basis set were chosen based on previous investigations,^{31, 34} and details of the calculations are given in Supplementary Information. The TD and CDD can help in visualizing the transition dipole distribution and the electron density difference between the excited state and the ground state upon excitation, respectively.³⁸⁻⁴⁰ The quantum chemical calculation of **1** was based on the structure resolved by Wang et al.³⁰ For computational efficiency, the phenyl group and partial pyridyl group were replaced by H to form $[\text{Au}_{20}(\text{PH}_3)_6(\text{PH}_2\text{py})_4\text{Cl}_4]^{2+}$ (**A2** in Fig. S1). The CDD and TD contours of the main transitions (shown in Supplementary Table S1) were constructed based on the TD-DFT results. From the CDD, it is found that electrons are localized on outer ligands while holes are localized on the Au core, indicating intramolecular charge transfer (ICT) from the Au core to the outer phosphine ligands (metal to ligand charge transfer, MLCT). From the TD, it can be seen that all

excitations are delocalized over the entire cluster. Fig. S2 shows the highest occupied molecular orbital (HOMO) and the lowest unoccupied molecular orbital (LUMO) of **A2**. The density of the HOMO is mainly localized over the Au atoms while the density of LUMO is distributed over the cluster, including the pyridyl rings. This distribution of the molecular orbital supports the results of the CDD calculation, proving MLCT in the rod-shaped Au₂₀ cluster. As ICT is significantly sensitive to the surrounding solvents, the solvation that arose from solute–solvent interactions upon excitation could change the excited-state charge transfer dynamics.

3.3 Femtosecond Transient Absorption Measurements

Comparative ultrafast transient absorption measurements of cluster **1** were performed in methanol, ethanol and *n*-propanol. Fig. 2 shows the broadband transient absorption spectra of **1** at different delay times from 300 fs to 80 ps in these solvents after excitation at 400 nm. The transient spectra in all three solvents consist of ground-state bleaching (GSB) around 480 nm which resembles the inverted spectral profiles of the steady-state absorption (see Fig. 1a). Over the whole spectral region, broad excited-state absorption (ESA) signals are observed. As expected, the TA spectra exhibit solvent-dependent evolutions. During the measurement, the ESA around 550 nm undergoes a solvent-dependent blue shift with different time delays. To quantify the ESA peak shift dynamics of rod shaped Au₂₀ cluster in three solvents, we fitted transient absorption spectra at different time delays from 0.3 ps to 80 ps with Gaussian peaks (see Supplementary Fig.S3). The time dependent peak shift from the position at 0.3 ps can thus be calculated from the Gaussian peak position at different time delays. The resulting peak shift dynamics of **1** in three solvents are shown in Fig. 3a.

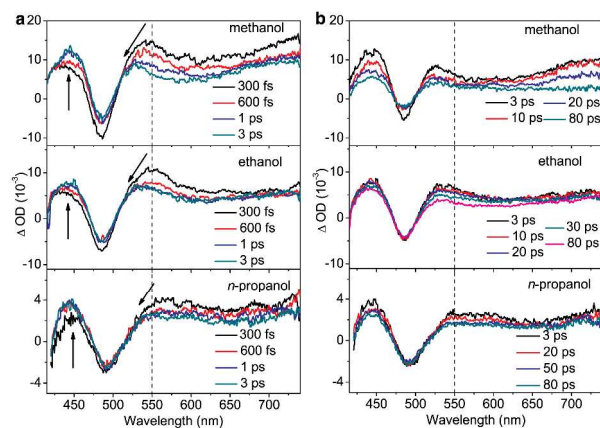


Fig. 2 Evolution of femtosecond transient absorption spectra. Spectra of **1** in methanol, ethanol, *n*-propanol measured with 400nm excitation and magic angle pump-probe polarization at different time delays. The spectral evolution is separated in two time domains 300 fs–3 ps (a), 3 ps–80 ps (b). The dashed line at 550 nm is a guide to the eye for identifying the spectral shift.

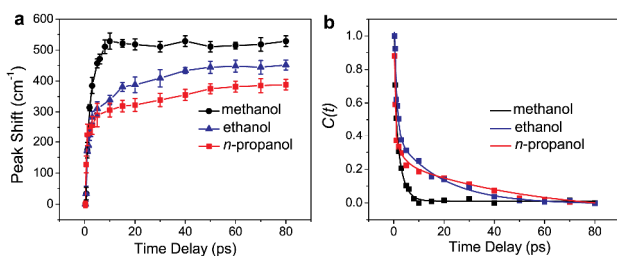


Fig. 3 (a) Peak shift dynamics; (b) excited-state peak shift time correlation functions, $C(t)$ and fits of 1 in three solvents.

The blue shift of ESA peaks in broad transient absorption spectra could arise from both vibrational relaxation and solvation. To figure out the origin, a peak shift correlation function is calculated by^{23, 41–43}

$$C(t) = \frac{\nu(\infty) - \nu(t)}{\nu(\infty) - \nu(0)} \quad (1)$$

where $\nu(t)$ represents the peak position of the ESA around 550 nm at a time delay t after excitation with $\nu(0)$ and $\nu(\infty)$ denoting the initial and final positions of the peaks, respectively. Due to limited time resolution, a direct determination of $\nu(0)$ is difficult. Instead, the peak position at 300 fs in *n*-propanol is used as $\nu(0)$ while $\nu(\infty)$ is fixed at the final peak position in each solvent. The resulting correlation functions for three solutions and fits using three exponentials are shown in Fig 3b. The fitting parameters are listed in Table 1. It is seen that the first component might belong to the vibrational cooling and/or inertial part of solvent response,^{23, 42, 44} and the slow components are mainly corresponding to the diffusive part of solvation, where the fitted time constant from the correlation functions are ~18.8 ps in ethanol and ~54 ps in *n*-propanol, much slower than that in methanol (4ps). Such slow components are finally related to the adsorbed solvent molecules around the excited Au₂₀ cluster surface. The peak shift dynamics suggests that solvation is much faster and more prominent in methanol than that in ethanol and *n*-propanol.

Table 1. Fitting parameters for the peak shift correlation function of **1** in three alcohols versus solvent parameters.

	methanol	ethanol	<i>n</i> -propanol
Δf^a	0.71	0.67	0.63
viscosity (cP) ^b	0.54	1.07	1.95
τ_1 (ps)	0.85 (90%)	1 (66%)	0.4 (74%)
τ_2 (ps)	4 (10%)	18.8 (34%)	3.2 (8%)
τ_3 (ps)			54 (18%)
$\langle \tau \rangle$ (ps)	1.2	7.0	10.2
$\langle \tau \rangle^*$ (ps) ^a	5	16	26

^aData taken from ref.²³ ^bData taken from ref.⁴⁵ Δf is the polarity index. All

correlation functions are fitted by three exponential decays:

$C(t) = a_1 \exp(-t/\tau_1) + a_2 \exp(-t/\tau_2) + a_3 \exp(-t/\tau_3)$ The average solvation

time is calculated by $\langle \tau \rangle = (a_1\tau_1 + a_2\tau_2 + a_3\tau_3) / (a_1 + a_2 + a_3)$

$\langle \tau \rangle^*$ is the average solvation time from ref.²³.

For exploring the solvent-dependent dynamics of the excited-state relaxation, global fitting procedure combined with singular value decomposition (SVD) was further employed to extract the time-dependent correlations and Evolution-Associated Difference Spectra (EADS) from the transient data. The spectra in the three solvents were fitted using a sequential model with three components (see Fig. 4a). The solvent-induced blue shift of ESA typically results from solvent stabilized ICT state (ICT' state) because solvation gradually lowers the excited-state potential energy surface.^{43, 46–48} Besides, the strong ESA around 550 nm is decayed to give rise to the ESA around 440 nm in all these solvents (see Fig. S4), suggesting the formation of long lived intermediate states. According to previous investigations, the last long lived component was assigned to the surface state arising from the surface ligands or the ligand/metal interface.^{13, 17, 26–28} Thus, these three components from the global fitting are assigned to ICT state, solvent stabilized ICT state (ICT')

and surface state, respectively. From methanol to *n*-propanol, with increasing the length of the alkyl chains (or viscosities) of the alcohols, the time constants of the second (10-16 ps) components decrease. In methanol, the relaxation time from ICT state to ICT' state (0.85 ps) obtained from global fitting agrees with the measured solvation time (1 - 4 ps) as shown in Table 1, thus the ICT state of the excited Au₂₀ cluster is almost fully solvated prior to moving toward the long-lived surface state (15.9 ps). Therefore, the solvent dipoles fully reorganized around the excited Au₂₀ cluster surface, which lower the energy of the ICT state to form the low-energy ICT' state. In contrast, the average solvation times of ethanol and *n*-propanol measured as 7 ps (or 18.8 ps of the slow diffusive solvation) for ethanol and 10.2 ps (or 54 ps of the slow diffusive solvation) for *n*-propanol (Table 1) are much longer, so that the ICT state of excited Au₂₀ cluster in ethanol or *n*-propanol is not fully solvated before evolving to the surface states (10 - 12 ps).^{42, 49, 50} As a result, the energy of the ICT' state in methanol could be equal to or slightly lower than that of the surface state, leading to a slower trapping time (15.9 ps) in methanol than that in ethanol (~12 ps) or *n*-propanol (~10 ps). Based on the above analysis, the relaxation pathway models of excited state **1** in three solvents are summarized in Fig. 4b. It is evidenced that the excited-state relaxation of excited Au₂₀ cluster is significantly modulated by the potential competition between the solvation and surface trapping.

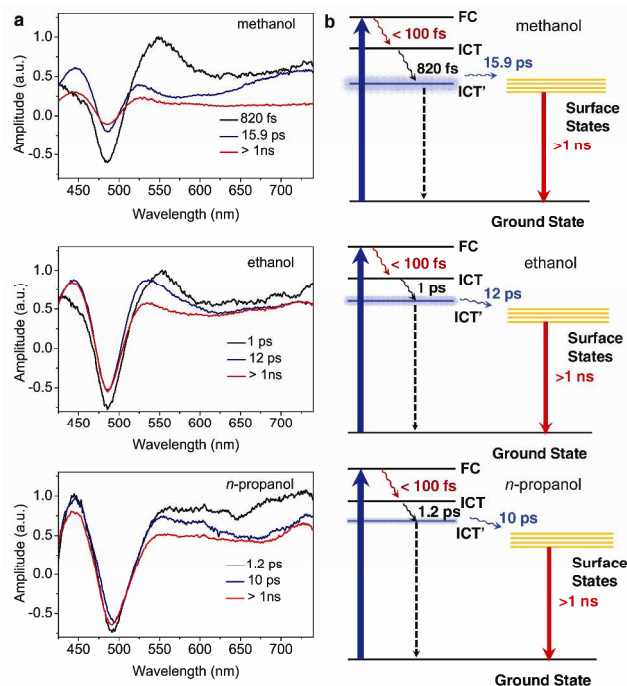


Fig. 4 Global analysis results and proposed relaxation pathways. (a) Evolution-associated difference spectra (EADS) and (b) relaxation pathway of **1** in three solvents based on singular value decomposition (SVD) combined with global fitting.

3.4 Oscillatory Features

Ultrafast excitation can also excite the acoustic vibration mode of AuNCs, while kinetic traces exhibit prominent oscillation during the initial time delay.^{13, 16-19} After a careful examination of the wavelength-dependent transient kinetics of the phosphine-protected Au₂₀ cluster in the three solvents, we observed oscillations only in methanol, whereas no obvious oscillatory features were observed for the transient kinetic traces of the phosphine-protected Au₂₀ cluster in ethanol or *n*-propanol. The different excited state relaxation

behaviors of **1** in the different alcoholic solvents could be due to the potential competition between solvation and surface trapping. This is interpreted by considering the solvation properties of these alcoholic solvents. The solvation (1 - 4 ps) of methanol is much faster than in the other two solvents (Table 1). Therefore, methanol molecules quickly rearrange and approach the excited cluster surface, forming a single layer solvent shell in a very short time (~1 ps) before excited Au₂₀ cluster moves to the surface trap state. While in ethanol and *n*-propanol, the solvation is so slow that excited Au₂₀ clusters are not fully solvated or even not solvated before evolving to the surface state so that there are fewer solvent molecules adsorbed around the cluster surfaces. Thus, there are two potential reasons why oscillations were not observed in ethanol or *n*-propanol. First, because the breathing vibration is relatively weak for very small Au clusters,⁵¹ the oscillation of **1** dissolved in ethanol and *n*-propanol is too weak to be seen. Second, for **1** in ethanol and *n*-propanol, the frequency of the breathing mode is higher (i.e., the oscillation period is shorter than the limited time resolution) due to the smaller total cluster size ($\omega \propto 1/R$).⁵² Accordingly, the oscillatory features may not have been resolved due to the limited time resolution (~90fs). In contrast, the observed oscillations in methanol suggested that the total cluster size of excited Au₂₀ increased by absorbing external methanol molecules around the excited cluster surface because of solvation,¹⁷ which lowers the oscillation frequency.

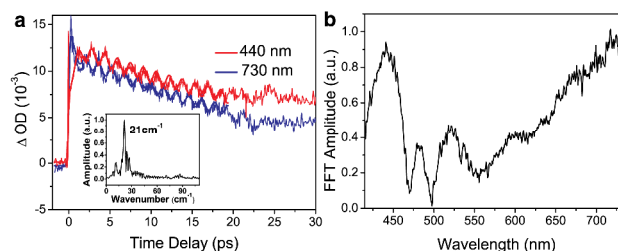


Fig. 5 (a) Transient kinetics and fitting around 440 nm and 750 nm in the initial 30 ps. The inset shows the Fourier transform of the kinetic traces around 440 nm. (b) Amplitude spectra of the oscillation at 21 cm⁻¹ based on the Fourier transform.

Regarding the observed oscillation of the phosphine-protected Au₂₀ cluster in methanol, in the 2D contour of the transient absorption spectra (see Fig. S5) the red to yellow part represents the ESA while the blue part stands for GSB. Modulation can clearly be seen around these peaks, where strong wavy features dominate down to about 20 ps after excitation. As these oscillations are superimposed on the transient signals, a standard fitting procedure is used to separate them.^{3, 53, 54}

$$\Delta A = A_0 \exp(-t^2 / 2\sigma^2) * [A_1 \exp(-t / \tau_1) + A_2 \exp(-t / \tau_2) \cos(\omega t + \phi) + A_3 \exp(-t / \tau_3)] \quad (2)$$

where σ is the width of the Gaussian impulsive pulse, ω and ϕ represents the frequency and phase of the oscillation, respectively, τ_1 and τ_3 stand for the excited state lifetimes. τ_2 is the damping time constant, reflecting the lifetime of the oscillation. The resulting damping time is 10 ps and the fitting results indicate that these oscillations have the same frequencies but opposite phases on the two sides of the GSB (see Fig. 5a). The phase shift indicates that the wavepacket motion of the excited population rather than impulsive resonant Raman process is responsible for modulating the transient absorption spectrum.^{55, 56} A Fourier transform of the data gives a frequency of 21 cm⁻¹ (see the inset of Fig. 5a) and no higher frequency oscillations were observed. Fourier transform of the transient data at all wavelengths were carried out to construct the

amplitude spectra of the oscillations (Fig. 5b). The main peaks are located around 440 nm and 700 nm, where the excited state absorptions are the strongest. The peak at 520 nm with a FT amplitude of ~ 0.5 is consistent with the ultrafast blue shift of the ESA from 550 nm to 520 nm due to solvation in methanol. Furthermore, the optically excited vibration of small Au clusters in the transient absorption measurement can be explained by dispersive excitation mechanism⁵⁷ which requires excitation of the symmetric breathing mode,^{16,57} and it is also excitation intensity independent as that in Au₂₀(SR)₁₆.¹⁷ In the calculated Raman spectra of **1**, it is found that the radial breathing mode of the cluster is located at 104.44 cm⁻¹ (see Fig. S6), much higher than the observed vibration frequency (~ 21 cm⁻¹). The lower frequency is from the increased mass of the oscillator due to the increase of methanol molecules adsorbed around the excited Au₂₀ cluster surface during solvation.

4. Conclusions

In summary, we have demonstrated that the excited state relaxation dynamics of rod-shaped phosphine-protected Au₂₀ clusters can be significantly modulated through the potential competition between solvation and surface trapping using femtosecond transient absorption experiments. The ultrafast ICT and solvation dynamics of the excited Au₂₀ cluster in three different alcoholic solutions are characterized. An optically excited radially symmetric vibration is observed only in polar methanol, with a frequency of 21 cm⁻¹ (0.62 THz). The relatively low frequency is due to the fast solvation which increased the mass of the oscillator. The solvation is relatively slow in less polar ethanol and *n*-propanol, so that the excited Au₂₀ cluster is not fully solvated before being trapped by the surface state where the vibration in these two solvents is too weak to be observed because fewer solvent molecules surround the cluster surface during the very slow solvation. These results provide a fundamental understanding of structure related ICT and solvation dynamics of ligand protected Au clusters and core/shell interactions in many other inorganic/organic complexes.

Acknowledgements

We thank Prof. Rongchao Jin for valuable suggestion and discussion. This work was supported by the 973 Program (2013CB834604), NSFCs (21173235, 91233107, 21127003, 21333012 and 21373232) and the Chinese Academy of Sciences (XDB12020200).

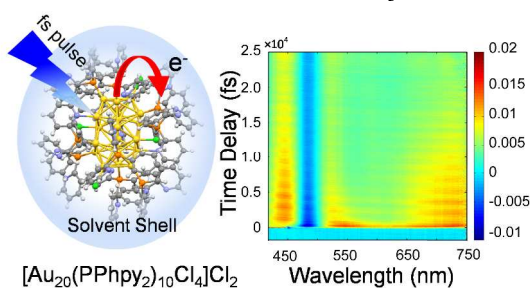
References

- P. D. Jadzinsky, G. Calero, C. J. Ackerson, D. A. Bushnell and R. D. Kornberg, *Science*, 2007, **318**, 430-433.
- H. Hakkinen, *Nat. Chem.*, 2012, **4**, 443-455.
- G. V. Hartland, *Chem. Rev.*, 2011, **111**, 3858-3887.
- J. F. Parker, C. A. Fields-Zinna and R. W. Murray, *Acc. Chem. Res.*, 2010, **43**, 1289-1296.
- G. Li and R. Jin, *Acc. Chem. Res.*, 2013, **46**, 1749-1758.
- J. Zheng, C. W. Zhang and R. M. Dickson, *Phys. Rev. Lett.*, 2004, **93**.
- C. Yi, M. A. Tofanelli, C. J. Ackerson and K. L. Knappenberger, Jr., *J. Am. Chem. Soc.*, 2013, **135**, 18222-18228.
- G. Ramakrishna, O. Varnavski, J. Kim, D. Lee and T. Goodson, *J. Am. Chem. Soc.*, 2008, **130**, 5032-5033.
- D. V. Talapin, J.-S. Lee, M. V. Kovalenko and E. V. Shevchenko, *Chem. Rev.*, 2009, **110**, 389-458.
- H. Qian, M. Zhu, Z. Wu and R. Jin, *Acc. Chem. Res.*, 2012, **45**, 1470-1479.

- J. F. Parker, K. A. Kacprzak, O. Lopez-Acevedo, H. Hakkinen and R. W. Murray, *J. Phys. Chem. C*, 2010, **114**, 8276-8281.
- G. Wang, T. Huang, R. W. Murray, L. Menard and R. G. Nuzzo, *J. Am. Chem. Soc.*, 2005, **127**, 812-813.
- S. A. Miller, J. M. Womick, J. F. Parker, R. W. Murray and A. M. Moran, *J. Phys. Chem. C*, 2009, **113**, 9440-9444.
- O. Lopez-Acevedo, K. A. Kacprzak, J. Akola and H. Hakkinen, *Nat. Chem.*, 2010, **2**, 329-334.
- S. H. Yau, O. Varnavski and T. Goodson, *Acc. Chem. Res.*, 2013, **46**, 1506-1516.
- O. Varnavski, G. Ramakrishna, J. Kim, D. Lee and T. Goodson, III, *ACS Nano*, 2010, **4**, 3406-3412.
- M. Zhou, S. Vdović, S. R. Long, M. Z. Zhu, L. Y. Yan, Y. Y. Wang, Y. L. Niu, X. F. Wang, Q. J. Guo, R. C. Jin and A. D. Xia, *J. Phys. Chem. A*, 2013, **117**, 10294-10303.
- H. Qian, M. Y. Sfeir and R. Jin, *J. Phys. Chem. C*, 2010, **114**, 19935-19940.
- M. Y. Sfeir, H. Qian, K. Nobusada and R. Jin, *J. Phys. Chem. C*, 2011, **115**, 6200-6207.
- M. S. Devadas, K. Kwak, J.-W. Park, J.-H. Choi, C.-H. Jun, E. Sinn, G. Ramakrishna and D. Lee, *J. Phys. Chem. Lett.*, 2010, **1**, 1497-1503.
- T. M. Carducci and R. W. Murray, *J. Am. Chem. Soc.*, 2013, **135**, 11351-11356.
- J. Huang, O. Buyukcakir, M. W. Mara, A. Coskun, N. M. Dimitrijevic, G. Barin, O. Kokhan, A. B. Stickrath, R. Ruppert, D. M. Tiede, J. F. Stoddart, J.-P. Sauvage and L. X. Chen, *Angew. Chem. Int. Ed.*, 2012, **51**, 12711-12715.
- M. L. Horng, J. A. Gardecki, A. Papazyan and M. Maroncelli, *J. Phys. Chem.*, 1995, **99**, 17311-17337.
- G. V. Hartland, M. Hu and J. E. Sader, *J. Phys. Chem. B*, 2003, **107**, 7472-7478.
- M. Walter, J. Akola, O. Lopez-Acevedo, P. D. Jadzinsky, G. Calero, C. J. Ackerson, R. L. Whetten, H. Groenbeck and H. Hakkinen, *Proc. Natl. Acad. Sci. U.S.A.*, 2008, **105**, 9157-9162.
- S. H. Yau, N. Abeyasinghe, M. Orr, L. Upton, O. Varnavski, J. H. Werner, H.-C. Yeh, J. Sharma, A. P. Shreve, J. S. Martinez and T. Goodson, III, *Nanoscale*, 2012, **4**, 4247-4254.
- M. S. Devadas, J. Kim, E. Sinn, D. Lee, T. Goodson, III and G. Ramakrishna, *J. Phys. Chem. C*, 2010, **114**, 22417-22423.
- S. A. Miller, C. A. Fields-Zinna, R. W. Murray and A. M. Moran, *J. Phys. Chem. Lett.*, 2010, **1**, 1383-1387.
- X. Li, M. Liang, A. Chakraborty, M. Kondo and M. Maroncelli, *J. Phys. Chem. B*, 2011, **115**, 6592-6607.
- X. K. Wan, Z. W. Lin and Q. M. Wang, *J. Am. Chem. Soc.*, 2012, **134**, 14750-14752.
- Y. Pei, Y. Gao, N. Shao and X. C. Zeng, *J. Am. Chem. Soc.*, 2009, **131**, 13619-13621.
- L. J. G. W. van Wilderen, C. N. Lincoln and J. J. van Thor, *PLoS One*, 2011, **6**, e17373.
- I. H. M. van Stokkum, D. S. Larsen and R. van Grondelle, *Biochimica et Biophysica Acta*, 2004, **1657**, 82-104.
- Y. Yuan, L. Cheng and J. Yang, *J. Phys. Chem. C*, 2013, **117**, 13276-13282.
- Z. Wu and R. Jin, *Nano Lett.*, 2010, **10**, 2568-2573.

36. A. Ojanperä, M. J. Puska and O. Lopez-Acevedo, *J. Phys. Chem. C*, 2013, **117**, 11837-11842.
37. J. M. Pettibone and J. W. Hudgens, *ACS Nano*, 2011, **5**, 2989-3002.
38. M. T. Sun, *J. Chem. Phys.*, 2006, **124**, 054903.
39. X. N. Ma, L. Y. Yan, X. F. Wang, Q. J. Guo and A. D. Xia, *Phys. Chem. Chem. Phys.*, 2011, **13**, 17273-17283.
40. L. Y. Yan, X. D. Chen, Q. G. He, Y. Y. Wang, X. F. Wang, Q. J. Guo, F. L. Bai, A. D. Xia, D. Aumiler, S. Vdovic and S. H. Lin, *J. Phys. Chem. A*, 2012, **116**, 8693-8705.
41. J. B. Asbury, Y. Wang and T. Lian, *Bull. Chem. Soc. Jpn.*, 2002, **75**, 973-983.
42. V. A. Lenchenkov, C. X. She and T. Q. Lian, *J. Phys. Chem. B*, 2004, **108**, 16194-16200.
43. M. Sajadi, M. Weinberger, H.-A. Wagenknecht and N. P. Ernsting, *Phys. Chem. Chem. Phys.*, 2011, **13**, 17768-17774.
44. X.-X. Zhang, M. Liang, N. P. Ernsting and M. Maroncelli, *J. Phys. Chem. B*, 2012, **117**, 4291-4304.
45. D. R. Lide, *CRC Handbook of Chemistry and Physics, 85th Edition*, CRC Press, Boca Raton, FL, 2004.
46. S. K. Pal and A. H. Zewail, *Chem. Rev.*, 2004, **104**, 2099-2123.
47. G. Ramakrishna and T. Goodson, III, *J. Phys. Chem. A*, 2007, **111**, 993-1000.
48. S. A. Kovalenko, J. Ruthmann and N. P. Ernsting, *Chem. Phys. Lett.*, 1997, **271**, 40-50.
49. E. Ishow, G. Clavier, F. Miomandre, M. Rebarz, G. Buntinx and O. Poizat, *Phys. Chem. Chem. Phys.*, 2013, **15**, 13922-13939.
50. L. Reynolds, J. A. Gardecki, S. J. V. Frankland, M. L. Horng and M. Maroncelli, *J. Phys. Chem.*, 1996, **100**, 10337-10354.
51. A. Tlahuice-Flores, R. L. Whetten and M. Jose-Yacaman, *J. Phys. Chem. C*, 2013, **117**, 12191-12198.
52. J. H. Hodak, A. Henglein and G. V. Hartland, *J. Phys. Chem. B*, 2000, **104**, 9954-9965.
53. N. Del Fatti, C. Voisin, F. Chevy, F. Vallee and C. Flytzanis, *J. Chem. Phys.*, 1999, **110**, 11484-11487.
54. K. Yu, P. Zijlstra, J. E. Sader, Q.-H. Xu and M. Orrit, *Nano Lett.*, 2013, **13**, 2710-2716.
55. C. J. Bardeen, Q. Wang and C. V. Shank, *J. Phys. Chem. A*, 1998, **102**, 2759-2766.
56. D. M. Sagar, R. R. Cooney, S. L. Sewall, E. A. Dias, M. M. Barsan, I. S. Butler and P. Kambhampati, *Phys. Rev. B*, 2008, **77**, 235321.
57. H. J. Zeiger, J. Vidal, T. K. Cheng, E. P. Ippen, G. Dresselhaus and M. S. Dresselhaus, *Phys. Rev. B*, 1992, **45**, 768-778.

Table of Contents Entry



Excited-state intramolecular charge transfer dynamics and coherent oscillation of ligand-protected rod shaped Au_{20} cluster was modulated through the competition between solvation and surface trapping.